Constitutive modelling of the strain-rate dependency of fabric reinforced polymers

Sylvain Treutenaere, Franck Lauro, Bruno Bennani, Grégory Haugou, Tsukatada Matsumoto, Ernesto Mottola

International Journal of Impact Engineering 108 (2017) 361–369

Constitutive modelling of the strain-rate dependency of fabric reinforced polymers

S. Treutenaere[a,*], F. Lauro[a], B. Bennani[a], G. Haugou[a], T. Matsumoto[b], E. Mottola[b]

[a] LAMIH, UMR CNRS 8201, Université de Valenciennes et du Hainaut-Cambrésis, CISIT, Mont Houy, F59313 Valenciennes CEDEX 9, France
[b] Toyota Motor Europe, Hoge Wei 33-Technical Center, Zaventem 1930, Belgium

* Corresponding author.
E-mail address: sylvain.treutenaere@univ-valenciennes.fr (S. Treutenaere).

ABSTRACT

Among the various mechanisms which occur during impact, the strain rate effect plays a significant role on the mechanical response of layered carbon fibre reinforced polymer structure. In this work, the viscoelastic behaviour of the material is studied to introduce a strain-rate dependency. To preserve numerical efficiency the generalised Maxwell model, formulated in the strain-space, is taken as a basis. The non-linear viscoelas-tic behaviour is introduced by coupling the generalised Maxwell model with a pre-existing intralaminar matrix continuum damage model. The fact that the Maxwell model preserves the explicit scheme of the damage model leads to an efficient material model for impact simulations. This paper proposes a complete framework to implement the strain-rate sensitive damage model in an explicit finite element code (for low-speed impact simulations). For this purpose, the procedure of parameter identification, based on Dynami-cMechanical Analysis, is given. Furthermore, a challenging experimental procedure on high-speed jack device with a particular attention paid to the consistency of the results is proposed to validate the devel-oped model.

Keywords: Composite, Textile, Damage, Strain rate, Large strain

1. Introduction

The use of Carbon Fabric Reinforced Polymers (CFRP) in the automotive industry increases significantly because of higher specific stiffness and strength and higher energy absorption compared to common metals. However the behaviour modelling, notably through the finite element method, is essential for their deployment on mass-product vehicles. This work is included in a wide project dedicated to simulate the behaviour of CFRP under low-speed impact, such as pedestrian impact, on non-structural components (engine bonnet, roof, door, etc.). It is focused on the modelling of the strain-rate sensitivity and its coupling to a pre-existing intralaminar damage model. The reinforcement damage, as well as the interlaminar matrix damage (so-called delamination) is not considered in the present study, even though needed for simulation of low-speed impact on the considered layered CFRP.

To introduce a strain-rate sensitivity for dynamic loading, phenomenological models exist and they describe empirically the dependence of the elastic modulus (and possibly also the damage evolution, the failure criterion, etc.) on the strain rate by polynomial or logarithmic functions [1,2]. However, these models may suffer of numerical instabilities during finite element analysis due to the difficulty to obtain a realistic instantaneous strain rate.

In the wide family of the viscoelastic models used to model strain rate sensitivity of the elastic behaviour, the rheological ones are the most simple ones. They are based on the combination of two basic components, a purely elastic spring (Hooke element) and a purely viscous damper (Newton element), connected in parallel and/or in series and lead to a linear viscoelasticity. General forms are given by the two generalised rheological viscoelastic models: the generalised Kelvin model and the generalised Maxwell model.

The generalised Kelvin model is well-adapted to a stress-space formulation of a constitutive model since the stress applied to each sub-element is equal to the total stress applied to the material. Instead, the generalised Maxwell model is preferred for strain-space formulations. These models are widely used in the commercial finite element analysis software but suffer two drawbacks. The first one is the use of a significant number of parameters. Second, as defined, these generalised rheological viscoelastic models are linear and cannot represent the non-linear viscoelastic behaviour of the fibre reinforced polymers.

Another group is the family of the spectral models. Compared to the previously mentioned generalised rheological models, the spectral models provide a continuous spectrum of the relaxation times. The number of parameters to identify is thus reduced without losing

DOI : 10.1016/j.ijimpeng.2017.04.010

accuracy for describing the viscous phenomena. By using a Gaussian description of the spectrum, Maire [3] introduces a spectral model for the fibre reinforced polymers. Thereafter, Rémy-Petipas [4], Schieffer et al. [5], Huchette [6], Berthe et al. [7] have gradually improved the model by introducing thermal effects and damage coupling. The spectral models expressed as such, however, are suffering substantial computational times in case of explicit simulation scheme.

Functional formulations are also used to describe time irreversibility problems. These formulations rely on the basis that the instantaneous response of a material depends on the loading history. Thus, the Boltzmann superposition principle can be applied to viscoelastic stress analysis problems. Initially using a linear creep compliance in the formulation, Lou and Schapery [8] introduced a non-linear viscoelastic formulation for the fibre reinforced polymers. This model was successfully used for various unidirectional composites [9–11] but essentially for creep simulations.

Other authors [12–14] use a functional formulation of the generalised Maxwell model introduced by Simo and Hughes [15] to model the behaviour of polymers or composites at high strain-rates. They introduce also a non-linear viscoelastic behaviour by coupling the damage and the viscoelasticity. This formulation is very attractive by its computational efficiency, notably in explicit finite element simulations, and its simple implementation. But by using a generalised Maxwell model as basis it always remains to identify many parameters.

Despite this, this last model is chosen as viscoelastic model in the present work by its attractiveness for impact simulations thanks to its explicit scheme. An explicit suitable damage model for the intralaminar damage of fabric reinforced polymers [16] is coupled with the viscoelastic model. The coupling, by its original formulation, preserves the explicit schemes of both viscoelastic and matrix damage model, while introducing non-linear viscoelasticity. Hence, the numerical efficiency of the complete model is preserved. In addition, the present paper suggests a complete framework dedicated to the implementation of the strain rate sensitivity to a given intralaminar damage model in an explicit finite element code. The identification procedure of the viscoelastic parameters is explained, the formulation in a discrete strain space for the finite element method is provided and finally, the challenging validation procedure is detailed.

In Section 2, the linear generalised Maxwell model is described, with the application of the Boltzmann superposition principle to obtain the constitutive equation. Then, a coupling with a matrix damage model [16] is proposed in the second section. Moreover, in a third section, the formulation of this model in the finite strain framework is discussed. The implementation of this newly formulated model into an explicit finite element code is given afterwards. The next section presents the parameter identification through straightforward Dynamical Mechanical Analysis. Finally, the model is validated by an experimental test campaign carried out on a high-speed hydraulic jack facility. The details of these tests are provided in a last section, with a particular attention to the scale effect, critical in the damage analysis of the fabric reinforced polymers due to substantial side effects.

2. Formulation of the constitutive model

2.1. Functional formulation of the generalised maxwell model

The generalised Maxwell model relies on the combination of only two basic elements: a spring called a Hooke element, and a dumper called a Newton element. By arranging these elements in series and in parallel according to a scheme given by the generalised Maxwell model, the model is able to describe the increase of the stiffness of polymers at increasing strain rates.

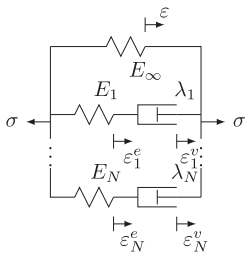

Fig. 1. Generalised Maxwell model.

To approach the real dynamic mechanical spectrum of the fibre reinforced polymers, the various relaxation times are introduced by using N Maxwell elements, made up a Hooke element and a Newton element in series, in parallel of the Hooke element (Fig. 1).

The strain ε applied to the generalised Maxwell model is equal to the strain applied to each branch (ε_j being the strain of the jth branch):

$$\varepsilon = \varepsilon_j = \varepsilon_j^e + \varepsilon_j^v \qquad \forall j \in [\![1, N]\!], \tag{1}$$

where the subscripts e and v are respectively relative to pure elastic and viscoelastic parts. The total stress is the sum of the stress applied to each branch:

$$\boldsymbol{\sigma} = \boldsymbol{\sigma}_\infty + \sum_{j=1}^{N} \boldsymbol{\sigma}_j, \tag{2}$$

where the subscript j indicates the properties of the jth Maxwell element. The stress at time t is then determined through the superposition theorem and is given by:

$$\boldsymbol{\sigma}(t) = \boldsymbol{\sigma}_\infty + \sum_{j=1}^{N} \boldsymbol{\sigma}_0 \cdot \exp\left(-\frac{t}{\tau_j}\right), \tag{3}$$

with $\tau_j = \frac{\lambda_j}{E_j}$ the relaxation time of the jth Maxwell element and leads to the relaxation modulus which is defined by: (Fig. 2)

$$E(t) = E_\infty + \sum_{j=1}^{N} E_j \cdot \exp\left(-\frac{t}{\tau_j}\right), \tag{4}$$

with E_j the elastic modulus of the jth Maxwell element. This expression of the relaxation modulus follows the form of Prony series.

To simplify the resolution of the differential equations, a single strain increment was considered as loading of the viscoelastic model and the relaxation stress response was described by introducing a relaxation modulus (Eq. (4)). But the response of the viscoelastic model has to be determined for random loading cases. The Boltzmann superposition principle suggests that the response of a material to a strain increment is independent of responses due to strain increments which have been previously initiated. Thus, let $\sigma_k(t)$ the stress at time t due to a strain increment $\Delta\varepsilon_k$ applied at a time ξ_k previous to t. By considering for example two strain increments, the total stress at time t can be obtained by superposition as follows:

$$\begin{aligned} \boldsymbol{\sigma}(t) &= \boldsymbol{\sigma}_1(t) + \boldsymbol{\sigma}_2(t) \\ &= E(t-\xi_1) \cdot \Delta\varepsilon_1 + E(t-\xi_2) \cdot \Delta\varepsilon_2. \end{aligned} \tag{5}$$

In a more general case, the total stress at time t is obtained by summing the effects of an infinite number of perturbations and is given by:

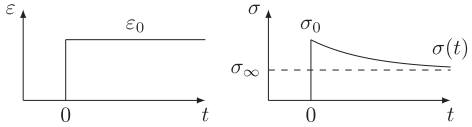

Fig. 2. Strain and stress histories of the Maxwell model in a relaxation test.

$$\begin{aligned}\boldsymbol{\sigma}(t) &= \int_{-\infty}^{t} E(t-\xi)\cdot \mathrm{d}\varepsilon(\xi) \\ &= \int_{-\infty}^{t} E(t-\xi)\cdot \frac{\mathrm{d}\varepsilon(\xi)}{\mathrm{d}\xi}\mathrm{d}\xi\end{aligned} \tag{6}$$

By replacing the relaxation modulus by the form of Prony series (Eq. (4)) obtained for a generalised Maxwell model, the total stress becomes:

$$\begin{aligned}\boldsymbol{\sigma}(t) &= \int_{-\infty}^{t} E(t-\xi)\cdot \frac{\mathrm{d}\varepsilon(\xi)}{\mathrm{d}\xi}\mathrm{d}\xi \\ &= \int_{-\infty}^{t} E_\infty \cdot \frac{\mathrm{d}\varepsilon(\xi)}{\mathrm{d}\xi}\mathrm{d}\xi \\ &\quad + \int_{-\infty}^{t} \sum_{j=1}^{N} E_j \cdot \exp\left(-\frac{t-\xi}{\tau_j}\right)\cdot \frac{\mathrm{d}\varepsilon(\xi)}{\mathrm{d}\xi}\mathrm{d}\xi \\ &= E_\infty \cdot \varepsilon(t) + \sum_{j=1}^{N} l_j(t)\end{aligned} \tag{7}$$

with

$$l_j(t) = \int_{-\infty}^{t} E_j \cdot \exp\left(-\frac{t-\xi}{\tau_j}\right)\cdot \frac{\mathrm{d}\varepsilon(\xi)}{\mathrm{d}\xi}\mathrm{d}\xi. \tag{8}$$

$l_j(t)$ represents the stress at time t on the jth Maxwell element of the generalised Maxwell model. It is coherent with the previous constitutive equation of the Maxwell element as the stress vanishes for an infinite time.

The Boltzmann integral is able to be applied to problems in three-dimensions. Consequently, by analogy with the previous uni-axial approach, the scalar values can be replaced by their tensor forms. Hence the total stress at time t results in:

$$\underline{\boldsymbol{\sigma}} = \underline{\underline{\mathbf{C}}}_\infty : \underline{\varepsilon}(t) + \sum_{j=1}^{N} \underline{\mathbf{l}}_j(t) \tag{9}$$

where

$$\underline{\mathbf{l}}_j(t) = \int_{-\infty}^{t} \underline{\underline{\mathbf{C}}}_j \cdot \exp\left(-\frac{t-\xi}{\tau_j}\right) : \frac{\mathrm{d}\underline{\varepsilon}(\xi)}{\mathrm{d}\xi}\mathrm{d}\xi. \tag{10}$$

$\underline{\underline{\mathbf{C}}}_\infty$ and $\underline{\underline{\mathbf{C}}}_j$ are respectively the fourth-order long-term stiffness tensor and the jth fourth-order viscoelastic stiffness tensor.

2.2. Viscoelasticity coupled with the matrix damage

The non-linear behaviour of the fibre reinforced polymers is now introduced through the coupling of the present viscoelastic model with an intralaminar matrix damage model.

The damage model, based on the Onera Damage Model [5,17–19], has been extended by Treutenaere et al. [16]. By considering privileged direction of matrix cracks, the model is able to consider the effect of the damage on the stiffness and physical phenomena due to the displacements of the crack lips. Crack closure effects (such as initial stiffness restoration), microscopic plasticity in the vicinity of the cracks leading to residual strain and friction mechanisms are examples of physical phenomena taken into account. The resulting constitutive relation is defined as follows:

$$\underline{\boldsymbol{\sigma}} = \underline{\underline{\widetilde{\mathbf{C}}}} : (\underline{\varepsilon} - \underline{\varepsilon}^0) - \underline{\underline{\mathbf{C}}}^0 : (\underline{\varepsilon}^{\mathrm{r}} + \underline{\varepsilon}^{\mathrm{s}} - \underline{\varepsilon}^0) \tag{11}$$

where $\underline{\underline{\widetilde{\mathbf{C}}}}$ and $\underline{\underline{\mathbf{C}}}^0$ are both fourth-order tensors which characterise the stiffness of the material.

While $\underline{\underline{\mathbf{C}}}^0$ denotes the elastic stiffness tensor of the material, $\underline{\underline{\widetilde{\mathbf{C}}}}$ represents the effective (damaged) stiffness tensor, evolving with the damage. $\underline{\varepsilon}^0$ represents the strain state where the cracks close off. It is due to the difference between the coefficients of thermal expansion of the matrix and of the reinforcement which creates residual stresses during the manufacturing and temperature variation.

Following the appearance of damage, the strains do not recover potentially their initial state when the stresses are relaxed. Some phenomena close to the cracks and which occur at a microscopic scale such as micro-plasticity or debris inside gaps may prevent a complete closure. These permanent strains are called the residual strain and are noticed $\underline{\varepsilon}^{\mathrm{r}}$. Their evolution is linearly dependant of the damage emergence.

The stored strain $\underline{\varepsilon}^{\mathrm{s}}$ can be regarded as representative of the position of the crack lips after closure. Therefore, this internal variable is used to introduced the energy stored but also dissipated by friction mechanisms during the damage emergence.

From this constitutive relation, it is convenient to define the driving strain $\underline{\varepsilon}^{\mathrm{h}}$. Physically it may be considered as the strain of the material reduced of the strains due to the crack lips sliding. By the following constitutive equation:

$$\begin{aligned}\underline{\boldsymbol{\sigma}} &= \underline{\underline{\widetilde{\mathbf{C}}}} : (\underline{\varepsilon} - \underline{\varepsilon}^0) - \underline{\underline{\mathbf{C}}}^0 : (\underline{\varepsilon}^{\mathrm{r}} + \underline{\varepsilon}^{\mathrm{s}} - \underline{\varepsilon}^0) \\ &= \underline{\underline{\widetilde{\mathbf{C}}}} \cdot \underline{\varepsilon}^{\mathrm{h}},\end{aligned} \tag{12}$$

the driving strain is thus given by:

$$\underline{\varepsilon}^{\mathrm{h}} = \underline{\varepsilon} - \underline{\underline{\widetilde{\mathbf{C}}}}^{-1} : \underline{\underline{\mathbf{C}}}^0 : (\underline{\varepsilon}^{\mathrm{r}} + \underline{\varepsilon}^{\mathrm{s}} - \underline{\varepsilon}^0) - \underline{\varepsilon}^0. \tag{13}$$

Then, the coupling between the functional formulation of the viscoelastic model and the interlaminar damage model is carried out by using the effective stiffness tensor $\underline{\underline{\widetilde{\mathbf{C}}}}$ as long-term stiffness tensor of the generalised Maxwell model and by applying the driving strain $\underline{\varepsilon}^{\mathrm{h}}$. Therefore, the constitutive equation of the strain-rate sensitive damage model for the fabric reinforced polymers results in:

$$\underline{\boldsymbol{\sigma}} = \underline{\underline{\widetilde{\mathbf{C}}}} : \underline{\varepsilon}^{\mathrm{h}}(\mathrm{t}) + \sum_{\mathrm{j}=1}^{\mathrm{N}} \underline{\mathbf{l}}_{\mathrm{j}}(\mathrm{t}) \tag{14}$$

where

$$\underline{\mathbf{l}}_j(t) = \int_{-\infty}^{t} \underline{\underline{\mathbf{C}}}_j \cdot \exp\left(-\frac{t-\xi}{\tau_j}\right) : \frac{\mathrm{d}\underline{\varepsilon}^{\mathrm{h}}(\boldsymbol{\xi})}{\mathrm{d}\xi}\mathrm{d}\xi. \tag{15}$$

3. Extension of the constitutive viscoelastic model in finite strain

The formulation of a viscoelastic model in a total Lagrangian framework have been studied extensively [15,20]. In previous work, Flory [21] introduced the volumetric and deviatoric multiplicative split. It relies on the hypothesis that the viscoelastic volumetric and deviatoric responses are fully uncoupled. Kaliske [22] proposed an efficient formulation which separates the relaxation tensor, independent of the deformation, and the nonlinear elastic material tensor, expressed according to an hyperelastic formulation. It makes easier the parameter identification by fully uncoupling the elastic and the viscoelastic terms.

In this work, the damageable viscoelastic model is extended in finite strain by replacing the engineering strain tensor $\underline{\varepsilon}$ and engineering stress tensor $\underline{\boldsymbol{\sigma}}$ by respectively the Green-Lagrange strain tensor $\underline{\mathbf{E}}$ and the second Piola–Kirchhoff stress tensor $\underline{\boldsymbol{\Sigma}}$. This assumption was made for two reasons. Firstly, the maximal shear strain is less than 40% for the studied materials. Thus, the spurious softening which appears for compressive loading does not occur. Moreover, due to the small displacements in the fibre directions, the volumetric part of the strain tensor during the problematic large shearing can be neglected. The decomposition of the behaviour in volumetric and deviatoric components is therefore not essential. Also, in a layered composite structure under impact loading, pure large shear strain neither occurs in all plies and the structure will fail at small strain values.

Finally the constitutive relation in the finite strain framework is given by:

$$\underline{\underline{\Sigma}} = \underline{\underline{\underline{\underline{\widetilde{C}}}}} : \underline{\underline{E}}^{h}(t) + \sum_{j=1}^{N} \underline{\underline{I}}_j^m(t). \tag{16}$$

with

$$\underline{\underline{I}}_j^m(t) = \int_{-\infty}^{t} \underline{\underline{\underline{\underline{C}}}}_j \cdot \exp\left(-\frac{t-\xi}{\tau_j}\right) : \frac{d\underline{\underline{E}}^{h}(\boldsymbol{\xi})}{d\xi} d\xi \tag{17}$$

and

$$\underline{\underline{E}}^{h} = \underline{\underline{E}} - \underline{\underline{\underline{\underline{\widetilde{C}}}}}^{-1} : \underline{\underline{\underline{\underline{C}}}}^{0} : (\underline{\underline{E}}^{r} + \underline{\underline{E}}^{s} - \underline{\underline{E}}^{0}) - \underline{\underline{E}}^{0}. \tag{18}$$

4. Implementation in an iterative scheme

The numerical implementation of the viscoelastic model coupled with the matrix damage model into a finite element code is carried out by the calculation of the stress at time t_{n+1} with the knowledge of the strain at time t_n and the time increment $\Delta t_{n+1} = t_{n+1} - t_n$:

$$\underline{\underline{\Sigma}} = \underline{\underline{\Sigma}}\,\infty\,(t_{n+1}) + \sum_{j=1}^{N} \underline{\underline{I}}_j^m(t_{n+1}). \tag{19}$$

The long-term stress $\underline{\underline{\Sigma}}\,\infty\,(t_{n+1})$ is directly obtained by the explicit formulation of the matrix damage model. It therefore remains to determine the different viscous stress $\underline{\underline{I}}_j^m(t_{n+1})$. Using the previously established Boltzmann heredity integral and the additive properties of the integrals, the viscous stress at time t_{n+1} becomes:

$$\begin{aligned}\underline{\underline{I}}_j^m &= \int_0^{t_{n+1}} \underline{\underline{\underline{\underline{C}}}}_j \cdot \exp\left(-\frac{t_{n+1}-\xi}{\tau_j}\right) : \frac{d\underline{\underline{E}}^{h}(\boldsymbol{\xi})}{d\xi} d\xi \\ &= \int_0^{t_n} \underline{\underline{\underline{\underline{C}}}}_j \cdot \exp\left(-\frac{t_n + \Delta t_{n+1} - \xi}{\tau_j}\right) : \frac{d\underline{\underline{E}}^{h}(\boldsymbol{\xi})}{d\xi} d\xi \\ &\quad + \int_{t_n}^{t_{n+1}} \underline{\underline{\underline{\underline{C}}}}_j \cdot \exp\left(-\frac{t_{n+1}-\xi}{\tau_j}\right) : \frac{d\underline{\underline{E}}^{h}(\boldsymbol{\xi})}{d\xi} d\xi.\end{aligned} \tag{20}$$

Using the multiplicative of the exponential, the viscous stress at time t_{n+1} is expressed in function of the viscous stress at the precedent increment:

$$\begin{aligned}\underline{\underline{I}}_j^m &= \exp\left(-\frac{\Delta t_{n+1}}{\tau_j}\right) \cdot \underline{\underline{I}}_j^m(t_n) \\ &\quad + \int_{t_n}^{t_{n+1}} \underline{\underline{\underline{\underline{C}}}}_j \cdot \exp\left(-\frac{t_{n+1}-\xi}{\tau_j}\right) : \frac{d\underline{\underline{E}}^{h}(\boldsymbol{\xi})}{d\xi} d\xi.\end{aligned} \tag{21}$$

Since the problem discretisation relies on the transition between differential values and discrete times by the following relation:

$$\frac{d\underline{\underline{E}}^{h}}{dt} = \lim_{\Delta t_{n+1} \to 0} \frac{\underline{\underline{E}}^{h}(t_{n+1}) - \underline{\underline{E}}^{h}(t_n)}{\Delta t_{n+1}}, \tag{22}$$

and by integrating the previously established viscous stress at time t_{n+1} (Eq. (21)), the exact regressive formula for the current value of the viscous stress quantities is given by:

$$\begin{aligned}\underline{\underline{I}}_j^m &= \exp\left(-\frac{\Delta t_{n+1}}{\tau_j}\right) \cdot \underline{\underline{I}}_j^m(t_n) \\ &\quad + \underline{\underline{\underline{\underline{C}}}}_j \cdot \frac{1 - \exp\left(-\frac{\Delta t_{n+1}}{\tau_j}\right)}{\frac{\Delta t_{n+1}}{\tau_j}} : \left(\underline{\underline{E}}^{h}(t_{n+1}) - \underline{\underline{E}}^{h}(t_n)\right).\end{aligned} \tag{23}$$

Therefore, this viscoelastic model is set by N families of viscoelastic stiffness tensor $\underline{\underline{\underline{\underline{C}}}}_j$, related to a relaxation time τ_j provided as parameter. The viscoelastic tensor is given by using Voigt notation by:

Algorithm 1 Computation of the viscoelastic stresses.

Step 1. Calculation of the driving strain $\underline{\underline{E}}^{h}$ (Equation 13).

Step 2. Loading of the previous configuration $\underline{\underline{I}}_j^m(t_n)$ and $\underline{\underline{E}}^{h}(t_n)$.

Step 3. Calculation of the actual viscoelastic stress $\underline{\underline{I}}_j^m(t_{n+1})$ (Equation 23).

Step 4. Storage of the actual configuration $\underline{\underline{I}}_j^m(t_{n+1})$ and $\underline{\underline{E}}^{h}(t_{n+1})$.

Step 5. Addition of the actual viscoelastic stress to the infinite stress (Equation 19).

$$\underline{\underline{\underline{\underline{C}}}}_j = \begin{pmatrix} E^{ve}_{j(1)} & 0 & 0 & 0 & 0 & 0 \\ 0 & E^{ve}_{j(2)} & 0 & 0 & 0 & 0 \\ 0 & 0 & E^{ve}_{j(3)} & 0 & 0 & 0 \\ 0 & 0 & 0 & G^{ve}_{j(23)} & 0 & 0 \\ 0 & 0 & 0 & 0 & G^{ve}_{j(13)} & 0 \\ 0 & 0 & 0 & 0 & 0 & G^{ve}_{j(12)} \end{pmatrix} \tag{24}$$

where $E^{ve}_{j(i)}$ and $G^{ve}_{j(ik)}$ are parameters of the model.

The strain-space formulation of this viscoelastic model is very efficient in an explicit scheme because of the limitation of internal equilibrium loop. By using the strain field provided in finite element code in the material coordinate system and the viscoelastic stress at the previous time step, the actual viscoelastic stresses are updated. The details of the implementation procedure are given in Algorithm 1.

5. Identification procedure of the material parameters

5.1. Experimental procedure

The identification of the viscoelastic parameters is done by means of Dynamic Mechanical Analysis (DMA). Since the viscoelastic

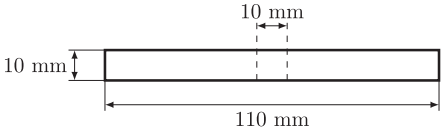

Fig. 3. DMA specimen geometry.

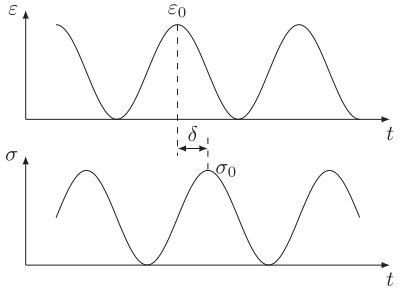

Fig. 4. Sinusoidal strain input and stress response of a visoelastic material.

constants are not dependent of the strains, they are determined through the study of small amplitude tensile experiments. The material remains in the elastic part and the identification of the normalised relaxation modulus can be determined without damage correction.

These tests are carried out at room temperature on an electromagnetic device (Instron E3000) whith a 3 kN load cell. The specimens are cut using the water-jet technique and their shape and dimensions are shown in Fig. 3. No heels are used since the deformation remains small and in order not to distort measurements. The distance between the clamps was set to 10 mm.

The Dynamic Mechanical Analysis are carried out by means of small amplitude cyclic tensile experiments. The cyclic deformation is introduced by the application of an imposed sinusoidal displacement with an angular frequency ω and an amplitude ε_0. In a permanent regime, the stress response of the material is sinusoidal with the same angular frequency as the one imposed for the strains. However, the stress output is not in phase with the strain input (Fig. 4).

By the ratio of stress and strain the complex modulus E^*, which is consequently frequency dependent, is obtained:

$$E^*(i\omega) = \frac{\boldsymbol{\sigma}_0}{\varepsilon_0} \exp(i\delta). \tag{25}$$

By considering the split of the complex modulus given by:

$$E^* = E' + iE'', \tag{26}$$

the storage and the loss modulus are thus defined by:

$$E' = \frac{\boldsymbol{\sigma}_0}{\varepsilon_0} \cos(\delta), \tag{27}$$

$$E'' = \frac{\boldsymbol{\sigma}_0}{\varepsilon_0} \sin(\delta). \tag{28}$$

The loss angle δ, defined as the ratio between the loss modulus and the storage modulus, namely:

$$\tan(\delta) = \frac{E''}{E'} \tag{29}$$

is representative of the viscous ability of the material. When the loss angle is null the material is purely elastic, whereas when δ tends towards $\frac{\pi}{2}$ the material is purely viscous.

The experiments were conducted at nine frequencies between 0.01 and 30 Hz. It was not possible to test materials for higher frequencies with the actual facility since the machine limitations were reached.

5.2. Identification of the viscoelastic constants

By using the constitutive relation between the infinitesimal strain and the infinitesimal stress for an uni-axial model (Eq. (6)) and the definition of an input sinusoidal strain in a complex form, the complex modulus is given by:

$$E^* = \int_0^\infty E(t) \cdot \exp(-i\omega t) \mathrm{d}t. \tag{30}$$

$E(t)$ is the linear relaxation modulus coming from the generalised Maxwell model and is formulated in terms of the Prony series (Eq. (4)). Consequently, and after decomposition of the complex modulus in real and complex parts, the storage and the loss modulus are therefore expressed as:

$$E'(\omega) = E_\infty + \sum_{j=1}^{N} E_j \frac{(\omega\tau_j)^2}{1 + (\omega\tau_j)^2}, \tag{31}$$

$$E''(\omega) = \sum_{j=1}^{N} E_j \frac{\omega\tau_j}{1 + (\omega\tau_j)^2}. \tag{32}$$

N couples of viscoelastic stiffness E_j and relaxation time τ_j are identified such that the average square deviation between the predicted moduli (by using Eqs. (31) and (32)) and the measured storage E'_{exp} and loss E''_{exp} moduli at M frequencies ω_k such as:

$$\min_{E_j,\tau_j} \sum_{k=1}^{M} \left[\left(\frac{E'(\omega_k)}{E'_{\text{exp}}} - 1 \right)^2 + \left(\frac{E''(\omega_k)}{E''_{\text{exp}}} - 1 \right)^2 \right] \tag{33}$$

is minimum.

5.3. Identification of the intralaminar matrix damage parameters

Because the matrix damage is only acting on the long-term stiffness tensor (Section 2.2) and not on the viscous terms, and as the viscous stiffness tensor and the relaxation times are identified in the elastic part of the behaviour, the coupling between the viscoelastic model and the intralaminar damage model does not affect the identification procedure of both models.

As a consequence, the intralaminar matrix damage parameters need to be evaluated after the identification of the viscoelastic parameters with the same procedure as described in Treutenaere et al. [16]. Nothing change, except the initial (visco)elastic parameters now provided by means of DMA.

6. Evaluation of the material model

6.1. Investigated materials

This section describes the ability of the material model to predict the dynamic behaviour of Carbon Fabric Reinforced Polymers made up with three various fabric preforms, namely a bi-axial non-crimp fabric (see Fig. 5), a 3K plain-weave woven (see Fig. 6) and a 12K plain-weave woven (see Fig. 7). The matrix material is an epoxy

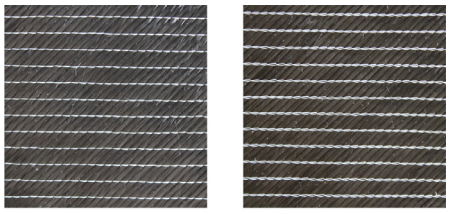

(a) Front side (b) Back side

Fig. 5. Overview of the non-crimp fabric preform.

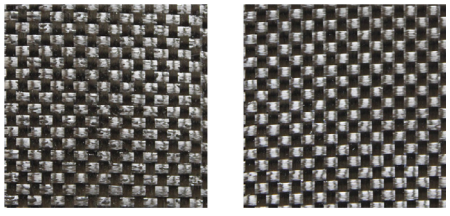

(a) Front side (b) Back side

Fig. 6. Overview of the 3K woven textile preform.

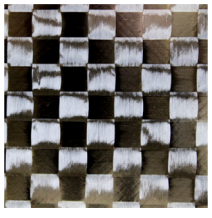

Fig. 7. Overview of the 12K woven textile preform.

Table 1
Viscoelastic parameters of the damageable viscoelastic model for the various fabric preforms. $G^{ve}_{i(12)}$ are expressed in MPa and τ_i in s.

Parameters	NCF	3K woven	12K woven
τ_1	100	100	100
$G^{ve}_{1(12)}$	351.19	325.46	164.55
τ_2	17.78	17.78	17.78
$G^{ve}_{2(12)}$	137.30	23.59	87.50
τ_3	3.16	3.16	3.16
$G^{ve}_{3(12)}$	174.22	103.30	155.00
τ_4	0.562	0.562	0.562
$G^{ve}_{4(12)}$	207.20	73.68	126.70
τ_5	0.1	0.1	0.1
$G^{ve}_{5(12)}$	122.60	84.74	109.6
τ_6	0.018	0.018	0.018
$G^{ve}_{6(12)}$	120.58	76.05	159.72
τ_7	0.00316	0.00316	0.00316
$G^{ve}_{7(12)}$	81.42	39.93	247.36

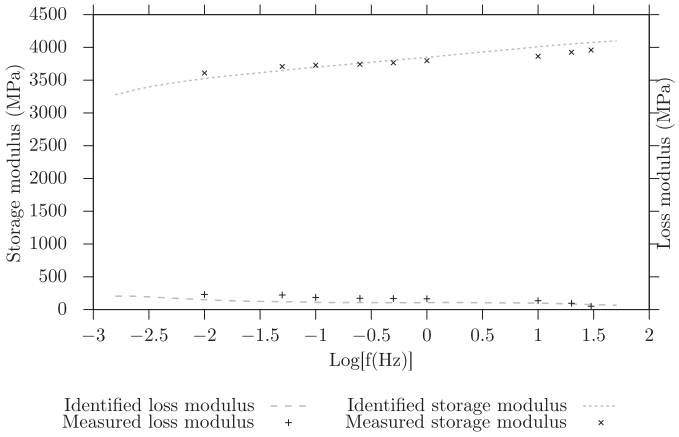

Fig. 8. Storage and loss modulus of biaxial non-crimp based composite.

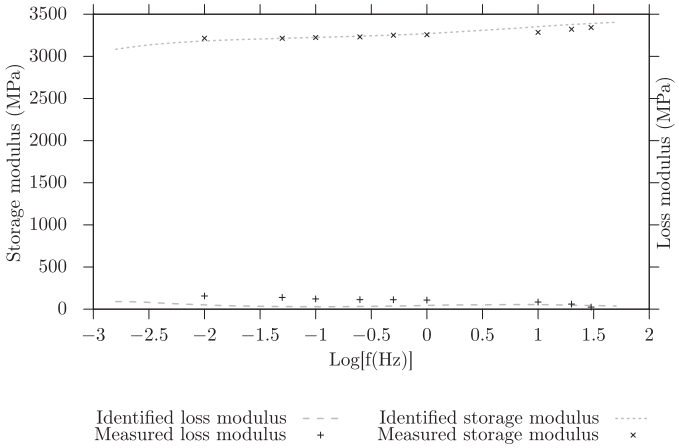

Fig. 9. Storage and loss modulus of 3K woven based composite.

resin coming from the polymerisation of the EPIKOTE™ 05475 by using the curative EPIKURE™ 05500.

The parameter identification of the viscoelastic model is carried out by using seven Maxwell elements. The optimisation procedures were carried out thanks to the commercial software Matlab® to minimise the Mean Square Error between the numerical and the experimental discrete relaxation spectra. As the storage modulii are much higher, and consequently being more influential on the mechanical response, than the loss modulii, the choice was done to better fit the evolution of the storage modulii.

The results of the parameter identification of the viscoelastic constants of the various CFRP are provided in Table 1 and Figs. 8 and 9.

The drop in loss modulus for frequencies greater than 10 Hz is not representative of the pure viscoelastic behaviour of the materials. In this frequency range, the specimens suffer from important self-heating. As a consequence, the identification could start to be not conservative for moderate high frequency. In order to precisely identify the viscoelastic parameters for frequencies reached in pedestrian impacts, the identification procedure still needs improvement. An investigated approach is to use the time-temperature equivalence to artificially reach higher strain-rate by cooling the material.

Table 2
Intralaminar matrix damage evolution parameters of the damageable viscoelastic model for the various fabric preforms – Part I.

Parameters	Units	NCF	3K woven	12K woven
$E^0_1 = E^0_2$	MPa	61,062	46,589	49,212
$\alpha_1 = \alpha_2$	MPa	277,722	147,722	286,678
ν_{21}	/	0.13	0.10	0.05
G^0_{12}	MPa	3000	3000	3000
g^{I}_{12}	MPa	0	1013	784
e^{I}_6	/	0	0.173	0.126
$b_1 = b_2$	/	0	0	0
$d^{\mathrm{nm}}_{c(1)} = d^{\mathrm{nm}}_{c(2)}$	/	0	0	0
$y^{\mathrm{nm}}_{0(1)} = y^{\mathrm{nm}}_{0(2)}$	/	0	0	0
$y^{\mathrm{nm}}_{c(1)} = y^{\mathrm{nm}}_{c(2)}$	/	0	0	0
$p^{\mathrm{nm}}_1 = p^{\mathrm{nm}}_2$	/	0	0	0
$d^{\mathrm{tm}}_{c(1)} = d^{\mathrm{tm}}_{c(2)}$	/	0.590	0.673	0.476
$y^{\mathrm{tm}}_{0(1)} = y^{\mathrm{tm}}_{0(2)}$	/	0.004	0.004	0.004
$y^{\mathrm{tm}}_{c(1)} = y^{\mathrm{tm}}_{c(2)}$	/	0.735	0.876	0.032
$p^{\mathrm{tm}}_1 = p^{\mathrm{tm}}_2$	/	0.260	0.107	0.416
$d^{\mathrm{tm}}_{c(3)}$	/	/	0	/
$y^{\mathrm{tm}}_{0(3)}$	/	/	0	/
$y^{\mathrm{tm}}_{c(3)}$	/	/	0	/
p^{tm}_3	/	/	0	/

Table 3
Intralaminar matrix damage evolution parameters of the damageable viscoelastic model for the various fabric preforms – Part II.

Parameters	Units	NCF	3K woven	12K woven
$h^{\mathrm{I}}_{m(1)} = h^{\mathrm{I}}_{m(2)}$	/	0	0	0
$h^{\mathrm{II}}_{m(1)} = h^{\mathrm{II}}_{m(2)}$	/	1	1	1
$h^{\mathrm{III}}_{m(1)} = h^{\mathrm{III}}_{m(2)}$	/	0	0	0
$d^{\mathrm{p}}_{c(3)}$	/	/	0.386	0.220
$y^{\mathrm{p}}_{0(3)}$	/	/	5.128	5.483
$y^{\mathrm{p}}_{c(3)}$	/	/	49.387	22.740
p^{p}_3	/	/	1.738	1.465
$h^{\mathrm{p}}_{m(3)}$	/	/	1	/
$\zeta_1 = \zeta_2$	/	0	0	0
ζ_3	/	/	0	/

Table 4
Intralaminar matrix damage friction parameters of the damageable viscoelastic model for the various fabric preforms.

Parameters	Units	NCF	3K woven	12K woven
$m^0_1 = m^0_2$	/	0.004	0.016	0.005
$m^m_1 = m^m_2$	/	26.115	6.129	19.220
m^0_3	/	/	0.164	0.063
m^m_3	/	/	100.00	61.12
$e^0_1 = e^0_2$	/	0.01	0.01	0.01
$a^{\mathrm{m}}_1 = a^{\mathrm{m}}_2$		/ 0	0	0
e^0_3	/	0.01	0.01	0.01

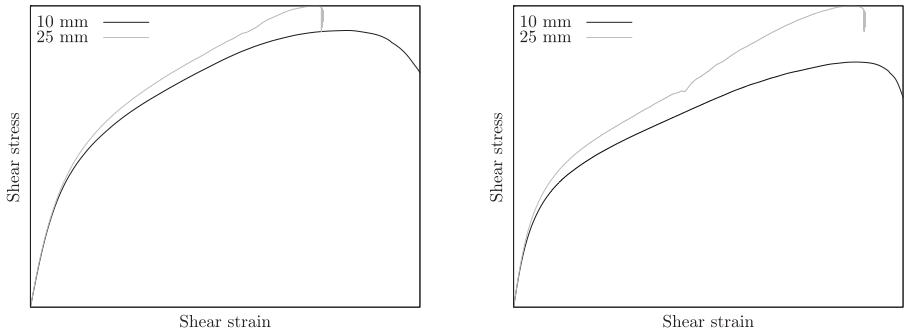

(a) Biaxial non-crimp fabric (b) 3K woven fabric

Fig. 10. Highlighting of the scale effect by the evolution of the specimen responses on tensile tests at 45° according to the fibre direction. Two different specimen widths have been tested: 10 mm and 25 mm.

The re-evaluated matrix damage parameters [16] are given in Tables 2–4.

The frequency range used for these DMA tests corresponds approximately to strain-rate from $1e^{-5}$ s^{-1} to 20 s^{-1}.

6.2. Tensile tests at different strain rates with standard specimens

In order to evaluate the ability of the model to represent the strain rate sensitivity of the CFRP, dynamic loading tests have been carried out at various strain rates. A hydraulic high speed device (Instron 65/20) with a 30 kN load cell is used for these tests. In order to ensure as much as possible a constant strain rate, the device is fitted with a piston system (Fig. 12). The piston stroke is used as slide during the acceleration phase of the hydraulic jack. At the end stroke, the translation speed, which reached a constant value, is transmitted to the piston.

Usually, specimens with reduced dimensions are used for dynamic testings. The dynamic facilities are not able to sustain the same maximal amount of force as the static ones. For this purpose, the specimen width is reduced to limit the specimen area. Furthermore, at constant loading speed the strain rate is artificially increased by reducing the specimen length.

Berthe [23] has shown that in case of fabric reinforced materials, the specimen length had to be at least two times greater than the specimen width. However the fabric reinforced polymers force to maintain a minimal width in order to present enough representative volume elements due to the roving size. An other aspect of the fabric reinforced polymers is critical in the choice of the coupon width: these materials show important edge damage and reduce the effective cross-section. If the ratio between the effective-cross section and the initial cross-section of the specimen is not at least those provided by standard coupons, the results become non-representative of the real material behaviour (Fig. 10).

Despite all the technical drawbacks, the dynamic specimens are designed to be identical to the coupons used for the standardised quasi-static in-plane shear tests (Fig. 11), which correspond to tensile tests at 45° according to the material direction, and are cut using the water-jet technique. Because of the original specimen dimensions for dynamic tests, none suitable clamping device were existing.

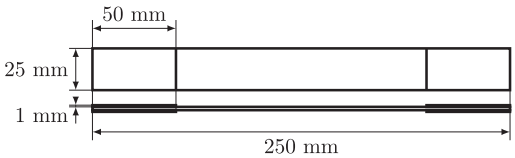

Fig. 11. Tensile specimen geometry.

Thus, as part of that work, a new clamping system has been designed. Three requirements specifications were formulated:

- to clamp standardised specimens;
- to apply homogenised clamp pressure in order to avoid a premature failure in the heels;
- to reduce the mass as much as possible in order to limit the inertial effects.

The adopted design solution consists of a prismatic clamping. The Computer-Aided-Design-based digital mock-up is shown Fig. 12. By screwing the external parts, namely the screw and the hood, the screw applies a pressure through the chocks on the clamp bottom surfaces inclined at 30°. Also, a pressure is applied by the hood on the clamp top surfaces. Hence, it results that homogeneous compressive forces are applied to the specimen heels.

According to experimental observations the strain rate sensitivity occurs mainly for shear loading in the material coordinate system (since the viscoelasticity of the resin is negligible when compared to the pure elastic stiffness of the fibres [24]) and due to the limitations of the hydraulic high speed device, only tensile tests at 45° according to the fibre directions are carried out. Except the speed loading, these dynamic tests are similar to the NF EN ISO 14,129 standard used to determine the in-plane shear properties of the composite materials. They are carried out at room temperature and at 3 speed loadings (1.7, 41 and 1000 mm s^{-1}) which correspond to approximate equivalent strain rates of 1 10^{-2}, 3 10^{-1} and 6.5 s^{-1}. Three coupons per speed loading are used to evaluate the repeatability of the results.

The results were conclusived as no heel fracture occurred. A moderate self-heating of the specimens has been observed at 1000 mm s^{-1}. For higher strain rates, the comparisons between experiments and simulations with non-thermal dependant models should be treated with caution.

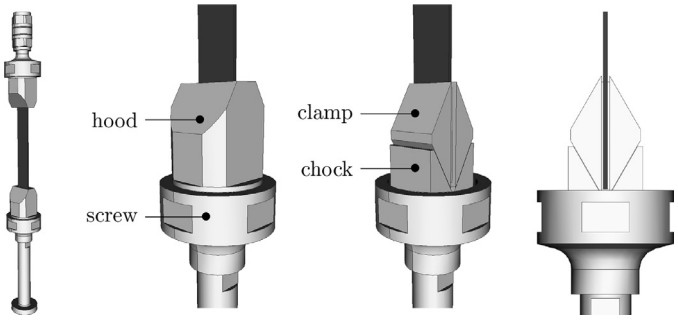

Fig. 12. Prismatic/screwing clamping system for dynamic tensile tests.

6.3. Comparison of the numerical model with the experiments

The present damageable viscoelastic model is implemented in FORTRAN 90 in a user material subroutine as described Section 4 for the explicit finite element code LS-DYNA®. Belytschko-Tsay shell elements with reduced integration are used for CFRP sections.

As validation procedure, the dynamic tensile tests (presented Section 6.2) and the quasi-static cyclic tensile tests (0.033 mm s^{-1}) at 45° according to the material direction, used to evaluate the in-plane shear properties, are simulated. Note that the cyclic tests are used to identify the matrix damage parameters. The hysteresis loop are due to both phenomena: friction of crack lips and viscoelasticity. however after parameter identification, the model predicts that most of the dissipated energy is due to the friction mechanisms. The tensile tests at 45° are used as validation tests of the viscoelastic part of the whole model since they are the most sensitive to the matrix viscoelasticity. Before comparing the numerical results with the experimental tests, some audits of the numerical model were carried out. Because of the sudden acceleration of the test device in dynamic loading case, the eigenfrequencies of the system are excited which can lead to a parasite noise in the measured response. Thus, a modal analysis of the system (high speed jack piston, clamping device, specimen and load cell) was made. The results demonstrate that the low eigenfrequencies (3.1 and 6.7 KHz) which may distort the force measurements are due to the mass of the clamping devices, the stiffness of the specimen and the piston. Thus, unlike the simulations of the quasi-static tests, the model simplification by applying directly the loading rate on the central parts of the specimen need to be verified. A first simulation of dynamic tensile loading at 45° according to the material direction at 1000 mm s^{-1}, which includes the piston, the clamping devices and a bi-axial non-crimp fabric specimen, has been carried out. The vibration predicted by the modal analysis occurs and leads to a slightly noisy response as expected. Another simulation have been carried out, but this time by imposing the measured strain-rate on the part of the specimen between the extensometer. The longitudinal displacement is therefore constrained with the measured values and the transverse displacement is free. After verification of the mesh convergence which occur with only one element since the deformation is homogeneous in this area, the force response of both simulations are then compared and the results are shown (Fig. 13). Note that the displacements are obtained by using a virtual extensometer in the middle of the specimen. Thus, the results are well compared in an area which is homogeneously deformed. The noise on the force response of the full device is not representative of the material behaviour. Therefore, and since the results are significantly close, the model reduction is validated. Therefore, the following simulations will be carried out on a single specimen.

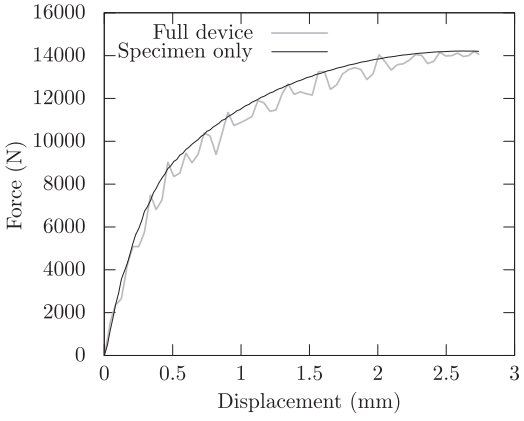

Fig. 13. Comparison of the force responses of a dynamic tensile tests at 45° according to the fibre direction given by a simulation where the full device is modelled, or by a simulation where only the coupon is considered.

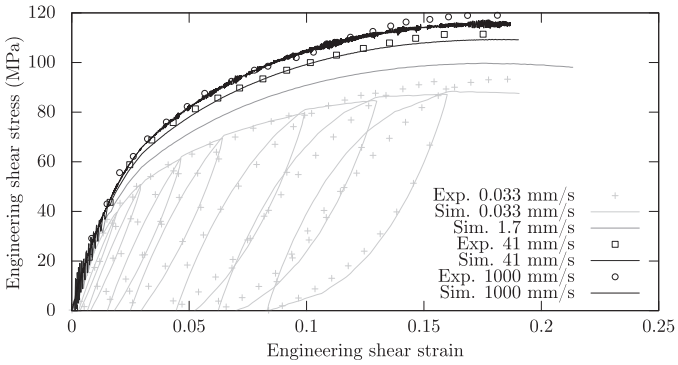

Fig. 14. Comparison between the experimental tests and the numerical modelling of tensile tests at 45° according to the fibre direction at various strain rates for the non-crimp fabric composite.

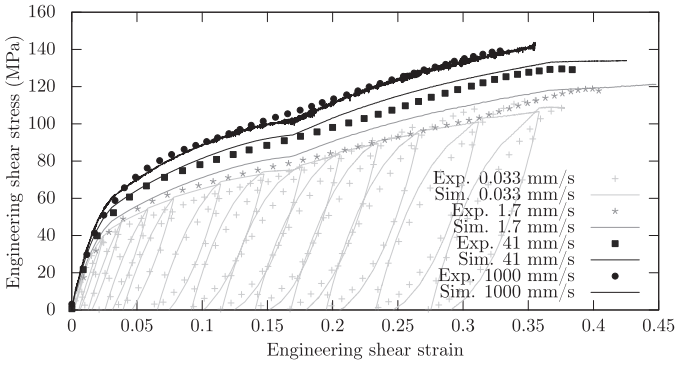

Fig. 15. Comparison between the experimental tests and the numerical modelling of tensile tests at 45° according to the fibre direction at various strain rates for the 3K woven fabric composite.

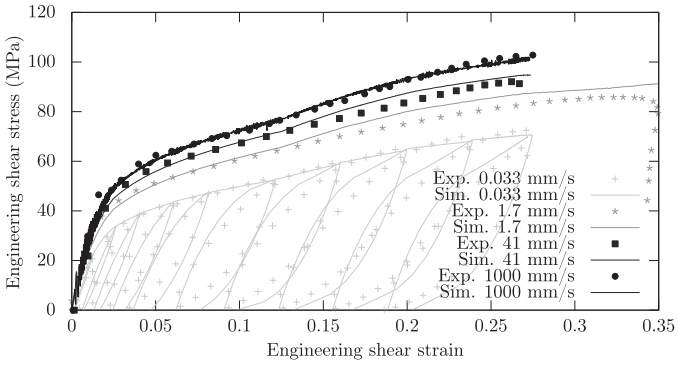

Fig. 16. Comparison between the experimental tests and the numerical modelling of tensile tests at 45° according to the fibre direction at various strain rates for the 12K woven fabric composite.

The results of the dynamic tensile tests at 45° according to the fibre direction carried out on three various fabric reinforced polymers are given Fig. 14 (bi-axial non-crimp fabric), Fig. 15 (3K woven fabric preform) and Fig. 16 (12K woven fabric preform). The oscillations on the numerical response at 1000 mm s^{-1} are due to the use of the real displacements of the hydraulic jack given by the experimental tests as input of the simulation. These displacements being noisy, the resulting responses are noisy too.

Also, it is essential to recall that the coupling between the viscoelastic model and the matrix damage model is done without additional parameter. Moreover, the parameters of both modules of the

model are identified independently: quasi-static cyclic tensile tests for the matrix damage and Dynamic Mechanical Analysis for the viscoelasticity. The viscoelastic parameters lead to an approximation of the real behaviour of the fabric reinforced polymers at various strain rate and need to be adapted for a good correlation with the experiments. The Dynamic Mechanical Tests are suffering of several drawbacks which can lead to the identification of non-representative parameters of the real strain-rate behaviour. The load capacity of the device is limited and the investigated materials are very stiff. Moreover, an important self-heating of the specimen occurs during DMA testing. Because of the epoxy response is temperature dependent, the identification may be distorted. By keeping in mind this context, the correlation between the experiments and the numerical model is good.

Due to a mistake in the calibration of the load cell, no data for the bi-axial non-crimp fabric material at 1.7 mm s^{-1} are available. Even so, the simulation response at this speed loading is plotted Fig. 14.

For the 3K woven fabric, the identification was more challenging. The quasi-static cyclic tensile tests at 45° according to the fibre direction used to identify the matrix damage were not carried out in the same period that the dynamic test campaign. Thus, as seen Fig. 15, the aging effect leads to a softening of the material and the experimental response at 1.7 mm s^{-1} is similar to the 0.033 mm s^{-1} response. A compromise was carried out during the identification procedure to obtain a acceptable distribution of the stress response according to the strain-rate.

7. Concluding remarks on the strain-rate dependency

The strain-rate sensitivity of the fabric reinforced polymers is greatly induced by the viscoelastic behaviour of the resin used as matrix. Among the various viscoelastic model, the generalised Maxwell model is used in the material law. This model offers the advantages of a very simple implementation into a finite element code, and most important a proved efficiency for explicit finite element simulations. Therefore, since the strain-rate dependency is essentially due to the matrix, the viscoelastic model is coupled with an intralaminar matrix damage model. This coupling is introduced by the definition of the driving strain, dependent on matrix damage, which acts on the generalised Maxwell model. The identification of the generalised Maxwell model is done by widespread Dynamic Mechanical Analysis. None additional parameter is needed for the coupling with the matrix damage.

This model is then validated through dynamic tensile tests at 45° according to the fibre direction by using an high-speed jack device. A new clamping system have been designed to allow dynamic tests on standardised coupons. Moreover, this clamping device avoids the premature failure in the heels. The simulations of the validation tests show good correlation on the various preforms.

The procedure for parameter identification of the viscoelastic model suffers of drawbacks. The facility used for DMA have a limited load capacity. Consequently, the frequency is limited to 30 Hz which restrained the identification of the viscoelastic spectrum to relatively low strain rates (less than 20 s^{-1}). However, for simulation of pedestrian impacts, the strain-rate range needs to be extended to approximately 100 s^{-1}. By using a time/temperature dependence, it could be possible to identify other parts of the spectrum. Also, this temperature dependence could be implemented directly in the viscoelastic model. In the future, another procedure to identify the viscoelastic parameters, such as creep tests or the SEÈ method which consists in plotting a three-dimensional surface given by the stress response and depending on the strain and the strain-rate, has to be investigated [25].

Acknowledgments

The present research work has been supported by International Campus on Safety and Intermodality in Transportation, the Region Nord Pas de Calais, the European Community, the Delegation Regionale a la Recherche et a la Technologie, the Ministere de l'Enseignement Superieur et de la Recherche, the Centre National de la Recherche Scientifique and TOYOTA MOTOR EUROPE: the authors gratefully acknowledge the support of these institutions.

References

[1] Daniel I, Werner B, Fenner J. Strain-rate-dependent failure criteria for composites. Compos Sci Technol 2011;71(3):357–64.
[2] Raimondo L, Iannucci L, Robinson P, Curtis PT. Modelling of strain rate effects on matrix dominated elastic and failure properties of unidirectional fibre-reinforced polymer-matrix composites. Compos Sci Technol 2012;72(7):819–27.
[3] Maire J-F. Études théorique et expérimentale du comportement de matériaux composites en contraintes planes. Besançon; 1992.
[4] Rémy-Petipas C. Analyse et prévision du comportement à long terme des composites fibres de carbone/matrice organique. These de doctorat, N o d'ordre 2000;801.
[5] Schieffer A, Maire J-F, Lévêque D. A coupled analysis of mechanical behaviour and ageing for polymer-matrix composites. Compos Sci Technol 2002;62(4):543–9.
[6] Huchette C. Sur la complé mentarité des approches expé rimentales et numé riques pour la modé lisation des mé canismes d'endommagement des composites stratifié s. Paris, France: Université Pierre et Marie Curie Thése de doctorat; 2005.
[7] Berthe J, Brieu M, Deletombe E. Thermo-viscoelastic modelling of organic matrix composite behaviour – application to t700gc/m21. Mech Mater 2015;81:18–24.
[8] Lou Y, Schapery RA. Viscoelastic behavior of a nonlinear fiber-reinforced plastic. Technical report. DTIC Document; 1970.
[9] Heil C, Cardon A, Brinson H. The nonlinear viscoelastic response of resin matrix composite laminates. Technical report. DTIC Document; 1984.
[10] Tuttle ME, Brinson HF. Prediction of the long-term creep compliance of general composite laminates. Exp Mech 1986;26(1):89–102.
[11] Zaoutsos SP, Papanicolaou GC, Cardon AH. On the non-linear viscoelastic behaviour of polymer-matrix composites. Compos Sci Technol 1998;58(6):883–9.
[12] Balieu R, Lauro F, Bennani B, Delille R, Matsumoto T, Mottola E. A fully coupled elastoviscoplastic damage model at finite strains for mineral filled semi-crystalline polymer. Int J Plast 2013;51:241–70.
[13] Dufour L, Bourel B, Lauro F, Haugou G, Leconte N. A viscoelastic-viscoplastic model with non associative plasticity for the modelling of bonded joints at high strain rates. Int J Adhesion Adhes 2016;70:304–14.
[14] Nciri M, Notta-Cuvier D, Lauro F, Chaari F, Maalej Y, Zouari B. Modelling and characterisation of dynamic behaviour of short-fibre-reinforced composites. Compos Struct 2017;160:516–28.
[15] Simo JC, Hughes TJ. Viscoelasticity. Computational inelasticity. Interdisciplinary applied mathematics. Springer New York; 1998. p. 336–73.
[16] Treutenaere S, Lauro F, Bennani B, Matsumoto T, Mottola E. Modelling of the intralaminar matrix damage with friction effects of fabric reinforced polymers. Compos Part B 2017;111:60–73.
[17] Chaboche J-L, Maire J-F. A new micromechanics based CDM model and its application to CMC's. Aerosp Sci Technol 2002;6(2):131–45.
[18] Huchette C, Lévêque D, Carrère N. A multiscale damage model for composite laminate based on numerical and experimental complementary tests. IUTAM symposium on multiscale modelling of damage and fracture processes in composite materials. Springer; 2006. p. 241–8.
[19] Marcin L. Modé lisation du comportement, de l'endommagement et de la rupture de maté riaux composites á renforts tissé s pour le dimensionnement robuste de structures. Ph.D. thesis; Université Bordeaux 1 2010.
[20] Le Tallec P, Rahier C, Kaiss A. Three-dimensional incompressible viscoelasticity in large strains: formulation and numerical approximation. Comput Methods Appl Mech Eng 1993;109(3):233–58.
[21] Flory PJ. Thermodynamic relations for high elastic materials. Trans Faraday Soc 1961;57(0):829–38.
[22] Kaliske M. A formulation of elasticity and viscoelasticity for fibre reinforced material at small and finite strains. Comput Methods Appl Mech Eng 2000;185(2–4):225–43.
[23] Berthe J. Comportement thermo-visco-élastique des composites cmo - de la statique á la dynamique grande vitesse. Ph.D. thesis; Ecole Centrale de Lille 2013.
[24] Nedjar B. A time dependent model for unidirectional fibre-reinforced composites with viscoelastic matrices. Int J Solids Struct 2011;48(16):2333–9.
[25] Lauro F, Bennani B, Morin D, Epee AF. The SEE method for determination of behaviour laws for strain rate dependent material: application to polymer material. Int J Impact Eng 2010;37(6):715–22.